Spatial Arrangement of Stormwater Infiltration Affects Subsurface Storage and Baseflow

Benjamin E. Choat, S.M.ASCE[1]; and Aditi S. Bhaskar, Ph.D.[2]

Abstract: Urban stormwater management is turning towards use of infiltration facilities, directing water that would have previously flowed overland into subsurface flow paths. Stormwater infiltration alters soil moisture, groundwater, and streamflow regimes, but it has been unclear how the spatial arrangement of infiltration-focused facilities affects catchment-scale water balances. This project used a physically based numerical model to investigate how spatial arrangements of infiltration facilities and subsurface media affects partitioning of water between unsaturated and saturated zones and baseflow duration and timing. More spatially distributed infiltration facilities, as compared to spatially clustered facilities, produced greater unsaturated zone storage, less saturated zone storage, and more total subsurface storage in scenarios where surface ponding was not severe. In silt, widespread surface ponding was observed. In sand, baseflow response to precipitation was delayed with clustered infiltration compared to distributed infiltration. These results can be used to guide decisions about how the spatial arrangement of stormwater infiltration facilities can affect urban catchment management goals, such as increasing plant available water and aquifer recharge or producing desired baseflow timing. **DOI: 10.1061/(ASCE)HE.1943-5584.0002005.** © *2020 American Society of Civil Engineers.*

Introduction

Urbanization impairs stream health by changing natural flow regimes, water quality, geomorphology, and ecological function and structure (Walsh et al. 2005). Conveyance-based stormwater management decreases the time to peak flow and increases the magnitude of peak flows and hydrograph recession rates, producing flashier hydrographs and altering catchment-scale water balances (Jefferson et al. 2017; Walsh et al. 2005). Water that once would have infiltrated into the ground, altering soil moisture, recharging aquifers, and slowly discharging as baseflow, defined here as groundwater-fed streamflow, is shifted to runoff.

Many approaches to reduce peak flows in urban streams use stormwater detention. Yet, even when peak flows are effectively managed, degradation of stream geomorphology, water quality, and stream ecology are still observed if the rest of the flow regime remains in an altered state (Jefferson et al. 2017; Poff et al. 1997; Walsh et al. 2005). Newer forms of stormwater management, called green infrastructure, are used to meet catchment management goals by incorporating harvest or infiltration of stormwater. Distributed harvest- or infiltration-based stormwater control measures (SCMs) reduce the volume of stormwater entering urban streams. Infiltrated water alters catchment water balances by routing stormwater into the subsurface increasing subsurface storage, which may drive catchment outputs via groundwater discharge to baseflow of local streams (Bhaskar et al. 2016a, b; Hamel et al. 2013; Hamel and Fletcher 2014; Jefferson et al. 2017; Newcomer et al. 2014; Price 2011). Alternatively, infiltrated stormwater may later be taken up by plants, and contribute to greater water availability and reduced irrigation requirements for semiarid plant growth (Shields and Tague 2015).

Unsaturated zone flow dynamics associated with subsurface media govern the translation of infiltration to recharge, but are commonly ignored due to difficulty in direct observations and computational demand required for unsaturated flow simulations However, in a three-dimensional setting, due to lateral flow and storage in the unsaturated zone, spatial arrangement of infiltration-based stormwater control measures (I-SCMs) in addition to the volume of stormwater received, may also affect recharge, subsurface storage, and baseflow. Ignoring or using 1D simplifications of unsaturated zone behavior or using saturated hydraulic parameters may be appropriate for averaged behavior over large spatial and temporal scales. However, over shorter time periods such as days or hours, and over smaller areas with nonuniform infiltration (e.g., small urbanized catchments), unsaturated zone dynamics likely play a significant role in modulating how infiltration is translated to recharge and baseflow (Staudinger et al. 2019; Woods et al. 1997). Furthermore, unsaturated zone dynamics can have direct and substantial effects on I-SCM performance. Winston et al. (2016) found that lateral exfiltration of water from I-SCMs to the surrounding unsaturated subsurface drove higher than expected drawdown rates in three Ohio I-SCMs. Elucidating relationships between unsaturated zone storage, saturated zone storage, recharge, baseflow, and the spatially explicit nature of stormwater infiltration therefore requires use of a variably saturated 3D approach.

Previous work connecting I-SCMs, groundwater recharge, and baseflow has been observational (Bhaskar et al. 2016b, 2018; Jefferson et al. 2017). In observational studies, the locations of I-SCMs cannot be moved while keeping all other catchment characteristics the same; therefore, observations are limited to comparisons between catchments with different I-SCM arrangement as well as differences in other catchment characteristics such as subsurface media. These studies do not allow for prediction of the effect of spatial arrangement of I-SCMs on unsaturated and saturated

[1]Graduate Research Assistant, Dept. of Civil and Environmental Engineering, Colorado State Univ., Fort Collins, CO 80523 (corresponding author). ORCID: https://orcid.org/0000-0002-7796-1323. Email: bchoat@rams.colostate.edu

[2]Assistant Professor, Dept. of Civil and Environmental Engineering, Colorado State Univ., Fort Collins, CO 80523. Email: aditi.bhaskar@colostate.edu

Note. This manuscript was submitted on April 16, 2019; approved on June 16, 2020; published online on August 31, 2020. Discussion period open until January 31, 2021; separate discussions must be submitted for individual papers. This paper is part of the ***Journal of Hydrologic Engineering***, © ASCE, ISSN 1084-0699.

zone dynamics or baseflow, preventing informed stormwater network design that aims to manage subsurface and baseflow hydrology (Bonneau et al. 2017).

On the other hand, distributed modeling approaches have the ability to isolate the effect of I-SCM spatial arrangement and capture physical catchment characteristics and spatially explicit features to which baseflow response is sensitive (Hamel et al. 2013). Previous work using distributed models to connect I-SCMs with groundwater or baseflow response has been limited to site-scale or local-scale groundwater response rather than the catchment-scale streamflow response (Endreny and Collins 2009; Li et al. 2017; Newcomer et al. 2014). Due to the spatially discrete nature of urban stormwater infiltration, the authors hypothesized that when discrete infiltration sites are spread over a greater area, larger lateral hydraulic gradients beneath I-SCMs form, resulting in significant lateral subsurface flow away from infiltration sites, decreasing episodic recharge and baseflow, and increasing storage.

The overarching goal was to gain insight into the general processes relating the arrangement of stormwater infiltration to subsurface storage and baseflow timing. To understand the dynamics of this relationship, the following questions were asked:

1. How does spatial arrangement of I-SCMs affect total subsurface storage, partitioning of storage between unsaturated and saturated zones, and episodic baseflow recession and timing?
2. How do different spatial arrangements impact the drivers of flow beneath infiltration facilities?
3. How do the effects of spatial arrangement of I-SCMs on subsurface storage and baseflow vary among different subsurface media?

A series of idealized simulations of distributed and clustered I-SCM spatial arrangements were executed for three different native subsurface media using an integrated surface-subsurface watershed model to answer these questions.

Methods

General Methodology

A physically based watershed model, ParFlow (Ashby and Falgout 1996; Jones and Woodward 2001; Kollet and Maxwell 2006; Maxwell 2013), was used to simulate idealized catchments with two spatial arrangements of I-SCMs. ParFlow models surface and subsurface flow by solving a kinematic wave approximation for overland flow implicitly coupled to Richards' equation, allowing for dynamic groundwater-surface water interactions (Kollet and Maxwell 2006). ParFlow was chosen because it allows for physically based representations of the hydrologic processes of infiltration, subsurface flow, and groundwater-surface water interactions, key to addressing this study's questions, whereas other models simplify one or more of these processes.

Model Domain Development

To isolate effects of spatial arrangement of I-SCMs, an idealized wedge-shaped urban catchment (Fig. 1) was simulated. The surface area of the domain was 0.25 km^2 (0.5 × 0.5 km) with a uniform thickness of 28 m. The computational grid was discretized to 5 × 5 m in the horizontal, resulting in 10,000 cells per layer. Variable vertical discretization was implemented with 14 layers representing a total thickness of 28 m, resulting in a total of 140,000 cells for the model domain. From top to bottom, the thickness of each layer of cells was 0.5, 0.5, 1, 1, 1, 1, 1, 1, 2, 2, 2, 5, 5, and 5 m. A terrain-following grid was used such that the angle of each surface cell was applied to all subsurface cells located below it (Maxwell 2013).

A digital elevation model (Fig. 1) was developed and used to generate the slopes that were an input into ParFlow. Then, a slope development routine (Barnes et al. 2016) was modified to set slopes of I-SCM cells to zero in both directions and stream cell slopes to zero in the direction perpendicular to streamflow. By assigning slopes of zero at I-SCM cells, water was only able to leave those cells through infiltration or evapotranspiration (ET). Specifying cells representing the stream to have zero slopes in the direction perpendicular to flow forced all flow to exit the domain at the outlet cell. Other than at I-SCMs, slopes parallel to streamflow (in the x-direction) were constant at 0.1%. Slopes perpendicular to streamflow (in the y-direction) were 0% in the row of stream cells, 25% in the cells adjacent to the stream (riparian cells), 15% along the row of impervious cells closest to the stream, and 5% throughout the rest of the domain other than at I-SCMs.

Physical Domain Properties

Representing a densely urbanized hillslope, all surface cells were defined as impervious except for I-SCM cells, riparian cells, and stream cells (Fig. 1). Impervious surfaces were represented by the top cell layer (0.5 m). I-SCMs were specified to be the top 1 m (two cell layers) of the domain. Stream and riparian cells were assigned a Manning's roughness coefficient of 4.05×10^{-7} $d/m^{1/3}$ (corresponding to 0.035 $s/m^{1/3}$ for natural streams and floodplains) and impervious cells a roughness coefficient of 3.5×10^{-7} $d/m^{1/3}$. While this value corresponds to 0.026 $s/m^{1/3}$, which is slightly rougher than common impervious surfaces, water was applied directly to I-SCMs, meaning there was effectively no overland flow on impervious areas in the model.

Subsurface properties were assumed to be homogeneous and isotropic and were defined using van Genuchten functions for the water retention curve and relative hydraulic conductivity [$k_r(\psi)$],

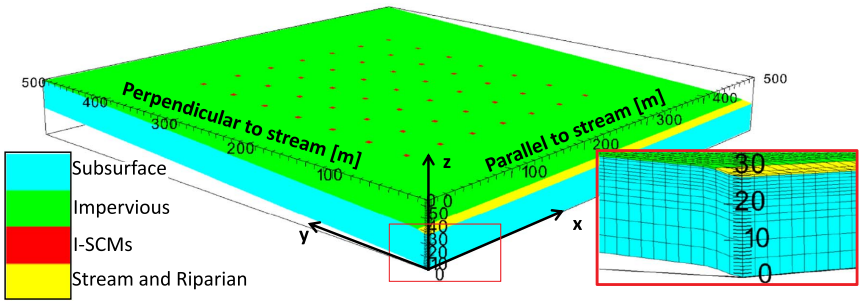

Fig. 1. Model domain with distributed I-SCM arrangement and cells shaded according to regions of the domain. Cutaway highlights terrain-following computational grid with variable vertical discretization. The stream outlet cell is at (0, 0, 28 m).

J. Hydrol. Eng., 2020, 25(11): 04020048

which depends on pressure head (ψ) (van Genuchten 1980; Maxwell 2013). Three subsurface media (silt, loamy sand, and sand) were simulated using saturated hydraulic conductivity (K_s) and van Genuchten parameters (α, n, θ_s, θ_r) obtained from ROSETTA (Schaap et al. 2001) (Table 1). A constant specific storage was applied in all scenarios (9.82×10^{-4} m^{-1}). Unsaturated parameters of impervious surface cells were based on concrete (Gupta et al. 2004) and saturated hydraulic conductivity of impervious cells was based on measurements conducted on fractured pavements (Wiles and Sharp 2008). I-SCM cells were assumed to have physical properties of sand.

Boundary Conditions

Boundary conditions along all subsurface boundaries (four sides and bottom of the domain) were no-flow boundaries since this study was only interested in fluxes out of the domain at the stream outlet (Kollet and Maxwell 2006). An overland flow boundary condition was implemented for the surface boundary, allowing spatially variable boundary conditions to be applied to individual surface cells [OverlandFlowPFB; (Kollet and Maxwell 2006)]. Annual precipitation was selected to represent a moderately humid climate (100 cm/year). Since streams are more likely to be gaining in humid areas, it was expected that these areas offer the most opportunity for spatially distributed I-SCMs to be effective at managing baseflow timing. Precipitation was applied to riparian and stream cells at the spin-up or transient precipitation rate (discussed in the following section). Below-average ET to precipitation ratios of 0.4, 0.081, and 0.0081 (Reitz et al. 2017) were used since development is likely to decrease ET. These scenarios are referred to as ET_{high} (0.4 = ET/P), ET_{mod} (0.081), and ET_{low} (0.0081) going forward. This resulted in annual ETs of 40, 8.1, and 0.81 cm/year, respectively. These ET rates were translated to volumes across the entire domain, and then applied equally to all pervious cells including I-SCM, riparian, and stream cells (i.e., impervious areas did not have ET).

Two spatial arrangements of I-SCMs were simulated and are referred to as clustered and distributed. Both arrangements had 49 total SCMs centered about the impervious area. Each I-SCM was represented as the size of a grid cell (5×5 m or 25 m^2). Forty-nine I-SCMs were distributed over 169 grid cells (49 SCMs/0.00423 km^2 or 11,597.6 SCMs/km^2) in the clustered scenario and over 3,025 grid cells in the distributed scenario (49 SCMs/0.0756 km^2 or 647.9 SCM/km^2) in 7×7 gridded patterns (Fig. 2). Overland routing of stormwater was not the focus of this study, and the numerical experiment was facilitated by equal stormwater volumes reaching each I-SCM. Therefore, the volume of rainfall over the entire impervious area was applied directly to I-SCM cells at a constant rate during each day of precipitation without a time delay. This ensured that all stormwater reached an I-SCM and each I-SCM received an equal volume of stormwater resulting in contributing areas of 5,000 m^2 for each I-SCM.

Table 1. Subsurface properties

Textural class	θ_r (–)	θ_s (–)	α (1/m)	n (–)	K_s (m/day)
Silt	0.05	0.489	0.66	1.68	0.44
Loamy sand	0.049	0.39	3.5	1.75	1.05
Sand	0.053	0.375	3.5	3.18	6.42
Impervious	0.094	0.23	1.9	1.59	1.00×10^{-3}

Note: θ_s = saturated soil moisture; θ_r = residual soil moisture; α = van Genuchten α; and n = van Genuchten n, saturated hydraulic conductivity K_s, specific storage for three soil types, and impervious cells.

This routing of rainfall to I-SCMs was carried out as a preprocessing step and was input into ParFlow using the OverlandFlowPFB surface boundary condition. While overland flow routing was not used to translate precipitation to I-SCMs, it was used within the stream and riparian cells where groundwater discharged as baseflow.

Spin-Up Simulations

The purpose of model spin-up is to allow modeled hydrologic conditions to reach equilibrium (i.e., steady state) with average climatic forcing. Constant forcing spin-up simulations were executed for each subsurface media and spatial arrangement of I-SCMs until daily changes in total, unsaturated zone, and saturated zone storages were all less than 0.01% of each respective storage. Simulations were executed until discharge was within 1% of daily inputs because at steady state, discharge would be equal to inputs as it was the only catchment output in spin-up simulations. The sand domain was simulated first as high conductivity aquifers were previously found to equilibrate faster than lower conductivity aquifers. Using the output from the constant forcing spin-up from the sand scenarios as initial conditions, both spatial arrangements were spun up for the loamy sand and silt scenarios. For the three ET scenarios, constant forcings of 0.329, 0.504, and 0.544 m/day were applied to

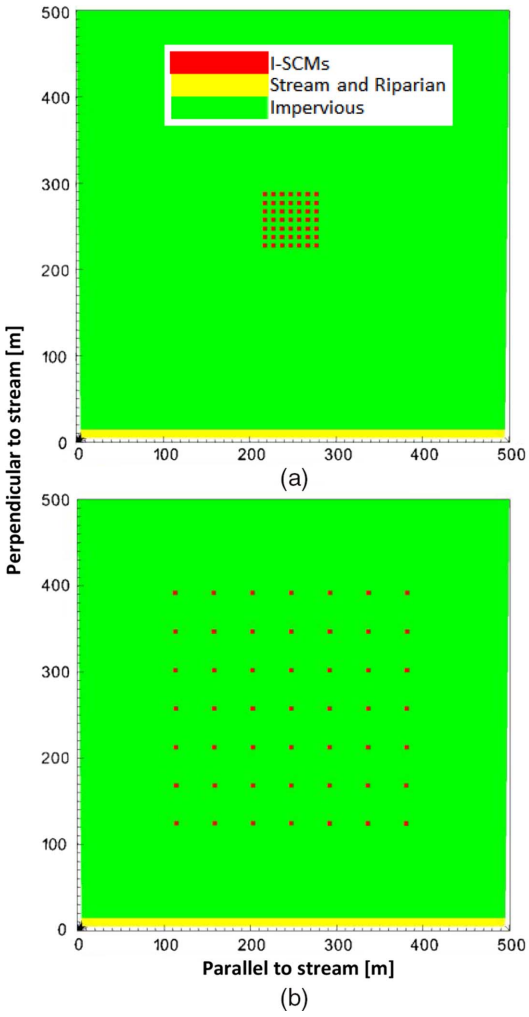

Fig. 2. Top-view of model domain showing (a) clustered; and (b) distributed spatial arrangements of I-SCMs. The origin (0,0) is the stream outlet of the model domain.

I-SCMs over time and which were equal to the volume of annual precipitation (100 cm/year) minus ET (40, 8.1, and 0.81 cm/year) over the entire impervious area. Net precipitation was applied to riparian and stream cells at a rate equal to daily precipitation minus daily ET (0.16, 0.25, and 0.27 cm/day).

Transient Simulations

After steady-state conditions were reached in spin-up simulations, this study simulated transient climatic forcings that varied the pattern of interevent durations, resulting in a variety of antecedent moisture conditions. As an example of computational time, to simulate 365 days of transient conditions on 20 processors, wall clock time was 1,833 h (i.e., 91.65 h elapsed real time) for the distributed sand scenario. Capturing the first 2.54 cm (1 in.) of run-off is a common SCM design standard (Jefferson et al. 2017). Therefore, the annual precipitation of 100 cm was applied over 40 day-long storm events that each had rainfall of 2.5 cm.

All precipitation over impervious cells was directly applied to I-SCMs such that each I-SCM received 125 m^3 (5 m) of water during each 1-day event. While the depth received is large, the volume is representative of infiltrated volumes in other studies (Bhaskar et al. 2018; Carleton 2010; Ferguson 1990; Sasidharan et al. 2019). By using larger but still realistic volumes of stormwater inputs, the authors were able to ensure that directional relationships between processes of interest were clear. Since antecedent moisture is an important driver of the processes governing the translation of infiltration to baseflow three interevent durations were applied in a varying order to produce different antecedent moisture conditions throughout the simulations. Interevent durations of 3, 14, and 21 days were chosen to generate varying antecedent moisture conditions while allowing for 40 precipitation events of 2.54 cm over a 365-day time period. The series in which the interevent durations were applied was 14, 3, 3, 14, 3, 3, 3, 21, 14, 3, 3, 14, 3, 3, 21, 3, 21, 3, 3, 14, 3, 3, 3, 14, 21, 3, 3, 14, 3, 3, 3, 14, 3, 21, 3, 14, 3, 3, 3, 14, and 4. It was assumed that ET occurring from impervious areas is negligible. Therefore, to maintain the catchment ET to precipitation ratios of 0.4, 0.081, and 0.0081, all ET (40, 8.1, and 0.81 cm/year; or 0.123, 0.0249, and 0.00249 cm/day, respectively) was applied evenly to pervious cells including I-SCMs, riparian, and stream cells. This translation of catchment-wide ET to these pervious areas meant that during each of the 325 days when precipitation was not occurring, ET was set to a rate of 4.943 cm/day (ET_{high}), 1 cm/day (ET_{mod}), or 0.1 cm/day (ET_{low}) at I-SCM, riparian, and stream cells. The ET_{high} value was chosen to maintain an overall catchment water balance at ET/P of 0.4, but this value was higher than I-SCM ET values reported in empirical studies, which ranged from about 0.125 to about 0.25 m/day of stormwater (based on I-SCM surface areas in this study) and about 0.09 to about 3 cm/day of ET (Denich and Bradford 2010; Hickman et al. 2011). ET_{mod} and ET_{low} values fell within these reported ranges but led to so little overall catchment ET and produced significant surface ponding with clustered I-SCMs, preventing our comparisons between I-SCM spatial arrangements.

General Calculations

To answer the research questions, analyses required calculations of stream discharge, subsurface storage, unsaturated zone storage, and saturated zone storage, as well as hydraulic conductivities, hydraulic gradients, and Darcy flow beneath I-SCMs. ParFlow outputs pressure heads at each grid cell and these pressure heads were used in postprocessing to calculate each of the above listed parameters.

Discharge, Q (m^3/day), at the catchment outlet cell was calculated using Manning's equation

$$Q_x = vA = -\frac{\sqrt{s_{o,x}}}{n} \times \Psi_s^{\frac{2}{3}} \times \Psi_s \times \Delta y = -\frac{\sqrt{s_{o,x}}}{n} \times \Psi_s^{\frac{5}{3}} \times \Delta y \quad (1)$$

where Q_x = discharge in x-direction out of domain (m^3/day), v = flow velocity (m/day) = $-\frac{\sqrt{s_{o,x}}}{n} \times \Psi_s^{\frac{2}{3}}$, A = cross-sectional area (m^2) = $\Psi_s \times \Delta y$, $s_{0,x}$ = bed slope in x-direction (–), n = Manning's roughness coefficient (day/$m^{1/3}$), Ψ_s = surface ponding depth, pressure head at outlet cell node (m), and Δy = grid-cell width in y-direction.

Subsurface storage, $V_{subsurf}$, included compressed and uncompressed storage terms and was calculated as

$$V_{subsurf} = \sum_{\Omega} [S(\psi) \times S_s \times \psi \times \Delta x \times \Delta y \times \Delta z + S(\psi) \times \phi \times \Delta x \times \Delta y \times \Delta z] \quad (2)$$

where Ω = cells of interest in the domain (i.e., all active cells or those with selected pressure heads), $S(\psi)$ = saturation as a function of pressure head (–), S_s = specific storage (1/m), ψ = pressure head (m), ϕ = porosity, Δx = grid-cell width in x-direction, and Δz = grid-cell width in z-direction. Eq. (2) was applied to the entire subsurface, resulting in total subsurface storage. In addition, saturated zone storage was calculated by applying Eq. (2) to grid cells with a pressure head greater than or equal to 0 m, and unsaturated zone storage was calculated by applying Eq. (2) to grid cells with a pressure head less than 0 m. To investigate subsurface flow beneath I-SCMs, hydraulic conductivities, hydraulic gradients, and Darcy flow between cells beneath I-SCMs and neighboring cells were computed. Weighted hydraulic conductivities were calculated as the harmonic mean of the hydraulic conductivity in the cell of interest and its neighboring cell of interest. The hydraulic gradients were calculated as the difference in hydraulic head between the cell of interest and the neighboring cell of interest. Gradients were defined such that a negative gradient is away from an I-SCM. The distance over which flow occurs, or in our case, the distance between cell centers, Δl, was defined such that a positive value is towards I-SCMs. Darcy flow between cells was then calculated as

$$q_x = -K_s \times k_r(\psi) \times \frac{\Delta(\psi + z)}{\Delta l} \quad (3)$$

where q_x = Darcy flow between cells in x-direction (m/day), $k_r(\psi)$ = relative hydraulic conductivity (–), $K_s \times k_r(\psi)$ = hydraulic conductivity (m/day), and $\Delta(\psi + z)/\Delta l$ = hydraulic gradient (m/m).

Analyses

For both spin-up and transient simulations, mass balances were calculated with Eqs. (1) and (2). To identify differences in subsurface drivers of flow between scenarios in the transient simulations, the 2.5 m under I-SCMs were analyzed for hydraulic conductivity and hydraulic gradient [Eq. (3)]. Ratios of lateral flow to vertical flow on a cell-by-cell basis were then calculated within the control volume defined by the horizontal size of each grid cell (5 × 5 m) and the 2.5 m beneath each I-SCM. For lateral flows beneath I-SCMs, vertical cell height was normalized by the smallest vertical discretization of 0.5 m. This was done so flow at larger cells would be weighted more than flow at smaller cells, since the volumetric flow at the same flux would be greater for larger cells (i.e., a 1-m vertical cell counted as two data points while a 0.5-m vertical cell counted as one). Darcy flow was calculated for the four lateral faces of each cell and the ratio of lateral flow to vertical flow was calculated for

each cell face (i.e., four ratios of lateral to vertical flow for each 0.5-m vertical span). It is also well understood now that I-SCMs may have significant effects on urban catchment hydrology (Ebrahimian et al. 2019), so volumes of plant available water in I-SCM cells and all cells within the layer just beneath the impervious layer (0.5–1.0 m depth), referred to here as the root zone, were compared on the wettest and driest days of the year. Plant available water was calculated for the 2 days by applying Eq. (2) to those cells where pressure head was equal to or less than field capacity (−3.4 m) and greater than wilting point (−153 m) (Dingman 2015).

Precipitation within the previous 15 days was calculated for each day of the transient simulations (after day 15) and was used to determine the wettest and driest days. Several days resulted in the same antecedent precipitation, so the wettest day was taken to be the day occurring farthest into the simulations that (1) had the most antecedent precipitation, and (2) was the day following a precipitation event. The driest day was taken to be the day occurring farthest into the simulations that (1) had the least antecedent precipitation, and (2) was the day preceding a precipitation event.

To characterize baseflow recession behavior between spatial arrangements and subsurface media, the authors compared the rate of change of discharge and the timing of maximum discharge between precipitation events. Rate of change of discharge was determined by comparing the discharge on the day after a precipitation event to the discharge the day before the following precipitation event. Then, to investigate effects of antecedent precipitation, defined here as precipitation depth in the previous 15 days, the rate of change and timing of maximum discharge were binned with depth of precipitation in the previous 15 days. To quantify and compare effects of I-SCM spatial arrangement on groundwater mounding, depth to water table (DTWT) on the wettest day was compared to DTWT on the driest day of the simulation.

Results

Spin-Up Mass Balance

The ET_{high} scenario is the only scenario that allowed for comparisons between I-SCM spatial arrangements and aquifer materials, and it was found the ET_{high} results were very representative of the ET_{mod} and ET_{low} results as well. So, this paper first discusses all results in terms of the ET_{high} scenario and then discusses differences between ET scenarios at the end of the results section. First, the effects of I-SCM spatial arrangement and subsurface media on the spin-up mass balance components (unsaturated, saturated, total subsurface, and surface storages; Table 2) were compared. Discharge was not considered since P-ET forcings were constant between scenarios leading to equal long-term average discharges.

Unsaturated storage was of similar magnitude for all subsurface media and I-SCM spatial arrangements (Table 2). In silt, clustered I-SCMs led to 30.9% more unsaturated storage than distributed I-SCMs. In contrast, distributed I-SCMs produced more unsaturated storage than clustered I-SCMs in the loamy sand (8.4% more) and sand (4.3%). With clustered I-SCMs, silt had the most unsaturated storage, whereas under distributed I-SCMs, silt had the least unsaturated storage.

Differences in saturated and total subsurface storage were larger between subsurface media than between I-SCM spatial arrangements. Silt had 41% more subsurface storage than loamy sand and 70% more subsurface storage than sand in both the clustered and distributed scenarios. Silt had 38% and 44% more saturated storage than loamy sand for clustered and distributed scenarios, and 73% and 69% more than sand for clustered and distributed scenarios, respectively. For loamy sand and sand, distributed I-SCMs had greater unsaturated storage and less saturated storage, whereas the opposite was the case for silt.

Silt had a large component of storage as surface storage, whereas sand and loamy sand did not. The surface storage in silt was a result of severe groundwater mounding that reduced infiltration capacity at I-SCMs and produced ponding over large portions of the impervious area where the groundwater mound reached the surface. By defining the I-SCMs to have zero slope, water that entered an I-SCM could only leave by infiltration or ET. While ponding occurred over a greater area under distributed I-SCMs, the total volume of surface ponding was 131% greater under clustered I-SCMs. Due to this surface ponding, the silt scenarios were not included in transient simulations.

Transient Mass Balance

Similar to spin-up, for transient simulations the differences in unsaturated storage between subsurface media were similar to differences between I-SCM spatial arrangements within a given subsurface media [Fig. 3(a)]. There was more unsaturated storage in the distributed scenarios compared to clustered scenarios

Table 2. Mass balance resulting from spin-up simulations

Mass balance component or comparison	Sand		Loamy sand		Silt	
	Clustered	Distributed	Clustered	Distributed	Clustered	Distributed
Unsaturated storage (m^3)	221,839	231,310	216,109	234,990	249,695	182,926
Difference (m)	−0.04		−0.08		0.27	
% difference	−4.2%		−8.4%		30.9%	
Saturated storage (m^3)	1,500,666	1,497,386	2,074,876	2,059,145	3,079,016	3,206,724
Difference (m)	0.01		0.06		−0.51	
% difference	0.2%		0.8%		−4.1%	
Subsurface storage (m^3)	1,722,505	1,728,695	2,290,984	2,294,135	3,328,710	3,389,651
Difference (m)	−0.02		−0.01		−0.24	
% difference	−0.4%		−0.1%		−1.8%	
Surface storage (m^3)	24	24	25	25	8,231	1,702
Difference (m)	0		0		0.03	
% difference	0.0%		0.0%		131.5%	

Note: The percent difference in storage between distributed and clustered arrangements for each soil type was calculated as $(V_2 - V_1) \Big/ \left(\frac{V_2 + V_1}{2}\right)$; V_2 = clustered I-SCMs; and V_1 = distributed I-SCMs.

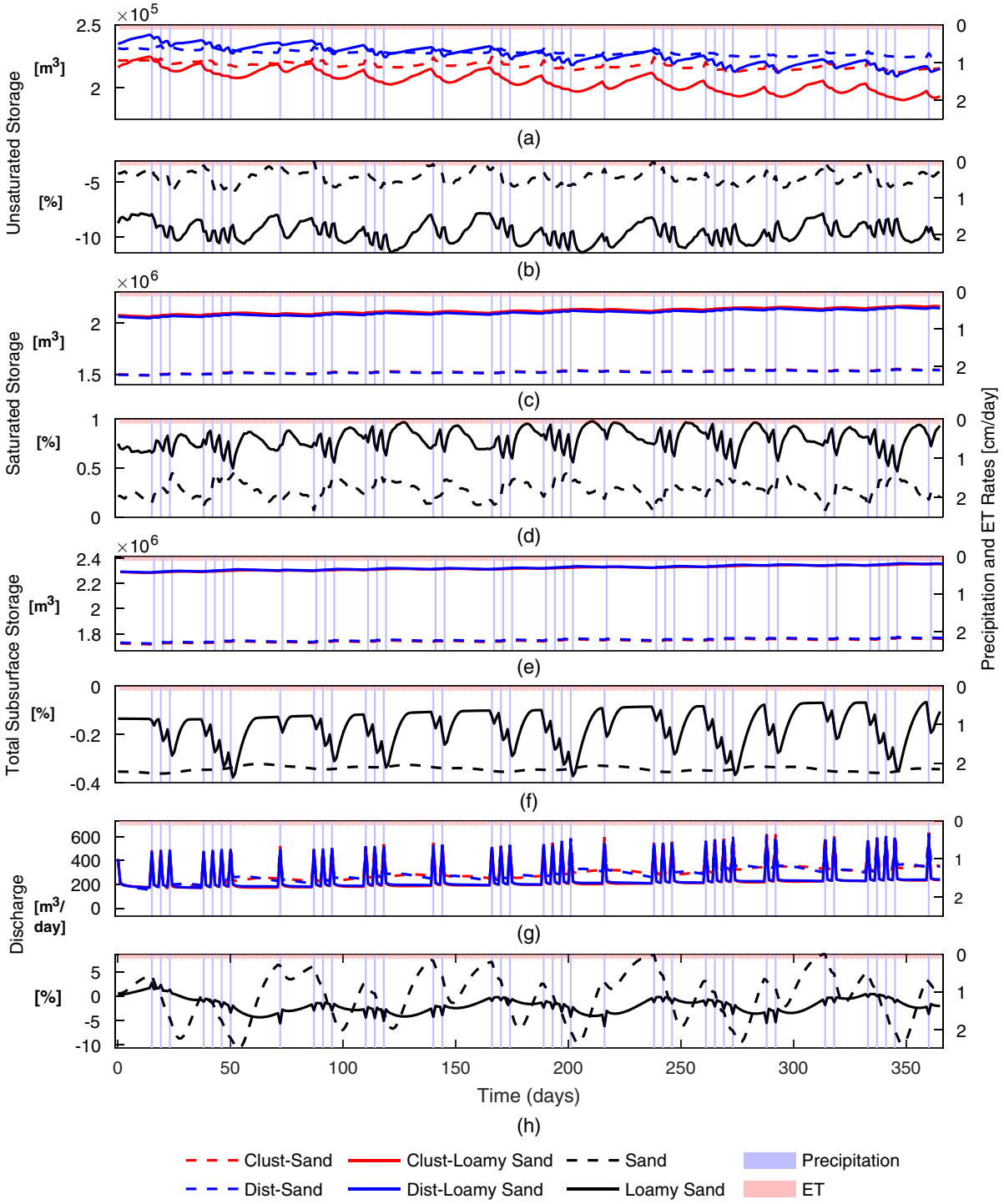

Fig. 3. (a) unsaturated storage; (b) differences in unsaturated storage between arrangements (clustered minus distributed, where positive indicates greater in clustered and negative indicates greater in distributed); (c) saturated storage; (d) differences in saturated storage between arrangements; (e) total subsurface storage; (f) differences in total subsurface storage between arrangements; (g) stream discharge; and (h) differences in discharge between arrangements. Note that the *y*-axes for (a–c, and e) do not start at 0.

throughout transient simulations [Fig. 3(b)]. This difference was larger for loamy sand (mean of 20,641 m^3, ~10%) compared to sand (mean of 10,250 m^3, ~5%). Unsaturated storage showed more temporal variability in loamy sand compared to sand, increasing between precipitation events as saturated storage drained. In general, unsaturated and saturated zone storages were more dynamic than total subsurface storage.

For saturated storage and total subsurface storage, the differences between spatial arrangements within each subsurface media were small compared to those between subsurface media [Figs. 3(c and e)]. Loamy sand had more saturated storage than sand (589,296 m^3 under clustered I-SCMs and 576,812 m^3 under distributed I-SCMs) and more total subsurface storage than sand (577,252 m^3 under clustered I-SCMs and 575,160 m^3 under

distributed I-SCMs). Saturated storage was consistently greater with clustered I-SCMs compared to distributed I-SCMs (on average 16,738 m^3, ~0.25% in loamy sand and 4,255 m^3, ~0.75% in sand). The larger unsaturated storage with distributed I-SCMs outweighed the smaller saturated storage, resulting in consistently greater total subsurface storage under distributed I-SCMs (3,902 m^3, ~0.35% in loamy sand and 5,995 m^3, ~0.2% in sand) [Fig. 3(f)].

Differences in discharge magnitude and behavior were larger between subsurface media than between I-SCM arrangements [Figs. 3(g and h)]. Sand had more discharge than loamy sand (69.4 m^3/day under clustered I-SCMs and 65.3 m^3/day under distributed I-SCMs on average). For loamy sand, discharge was similar between I-SCM arrangements. The sand scenario experienced greater variability in discharge over time and between spatial arrangements compared to loamy sand. During wet periods, baseflow was greater with distributed I-SCMs (~9% in sand, ~5% in loamy sand), while clustered I-SCMs produced greater baseflow during dry periods [Fig. 3(h)].

Discharge Recession

Discharge responses to precipitation were examined with the recession rate, or the rate of change of discharge during interevent periods. When there was more precipitation in the previous 15 days, the recession rate approached zero (Fig. 4). For loamy sand, the recession rate was similar between spatial arrangements [Figs. 4(a and b)]. In sand, the recession rate increased more strongly with antecedent precipitation in the clustered I-SCM compared to distributed I-SCM scenario [Figs. 4(c and d)] and distributed I-SCMs produced more consistent recession rates throughout the simulations. For loamy sand, the day after a precipitation event was always the day with the greatest baseflow between events [Figs. 5(a and b)]. In sand, the maximum baseflow occurred up to 15 days after a precipitation event [Figs. 5(c and d)]. In the clustered sand scenario, 9 of the 39 interevent durations experienced maximum baseflow 8–14 days after the precipitation event. Eight of those 9 interevent durations followed 5 cm or more precipitation during the previous 15 days. When there was 7.5 cm of antecedent precipitation, the maximum baseflow never occurred less than 12 days after a precipitation event [Fig. 5(c)]. Although delays in baseflow timing are difficult to directly observe in field studies, delayed baseflow can counteract the generally observed effect of urbanization to shorten recession times (Bhaskar and Welty 2015; Rose and Peters 2001). When compared to results from a study in Clarksburg, Maryland (Hopkins et al. 2020) that observed 171 out of 172 stream responses lasting less than 24 h, these delays in baseflow response are quite significant.

Depth to Water Table

Loamy sand had an overall shallower DTWT than sand (Fig. 6) (6.64 m versus 12.16 m on average). The shallowest DTWT was on the wet day with clustered I-SCMs and loamy sand, a case in which there was also surface ponding [Fig. 6(b); shown in white]. Infiltrated water affected DTWT over a greater area in the loamy sand scenario. In the sand scenario, both spatial arrangements were able to infiltrate all water without mounded water reaching the surface. Distributed I-SCMs maintained deeper average DTWT. Distributed I-SCMs also had deeper DTWT directly under I-SCMs in all scenarios except wet loamy sand, where all I-SCMs saturated under both arrangements [Figs. 6(b and d)]. Effects of I-SCM arrangement on plant available water was limited to areas near infiltration sites in sand, while effects were observed far from infiltration sites in loamy sand (Fig. S1). Also, in loamy sand, spatial patterns of plant available water varied greatly between I-SCM arrangements.

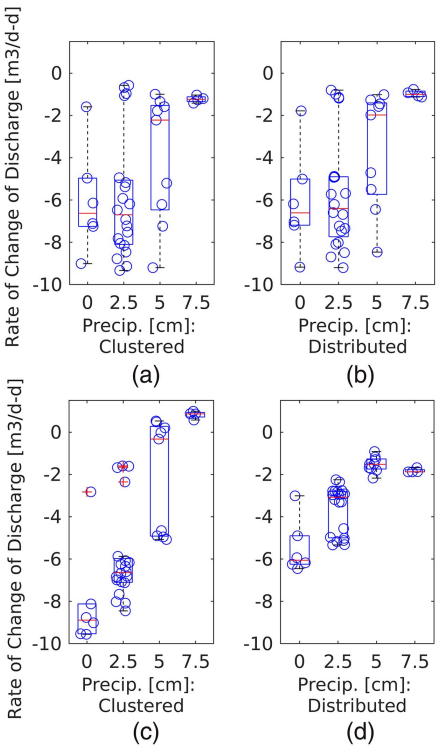

Fig. 4. Rate of change of discharge during interevent periods versus precipitation depth in the previous 15 days for (a) loamy sand clustered; (b) loamy sand distributed; (c) sand clustered; and (d) sand distributed.

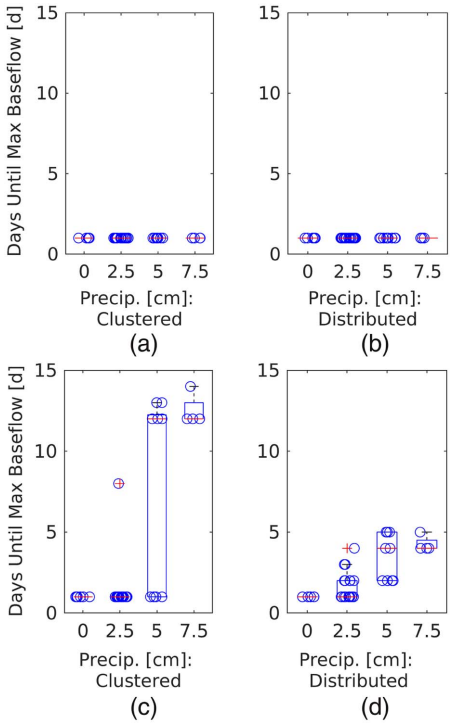

Fig. 5. Days after precipitation event until maximum baseflow versus precipitation depth in the previous 15 days for (a) loamy sand clustered; (b) loamy sand distributed; (c) sand clustered; and (d) sand distributed.

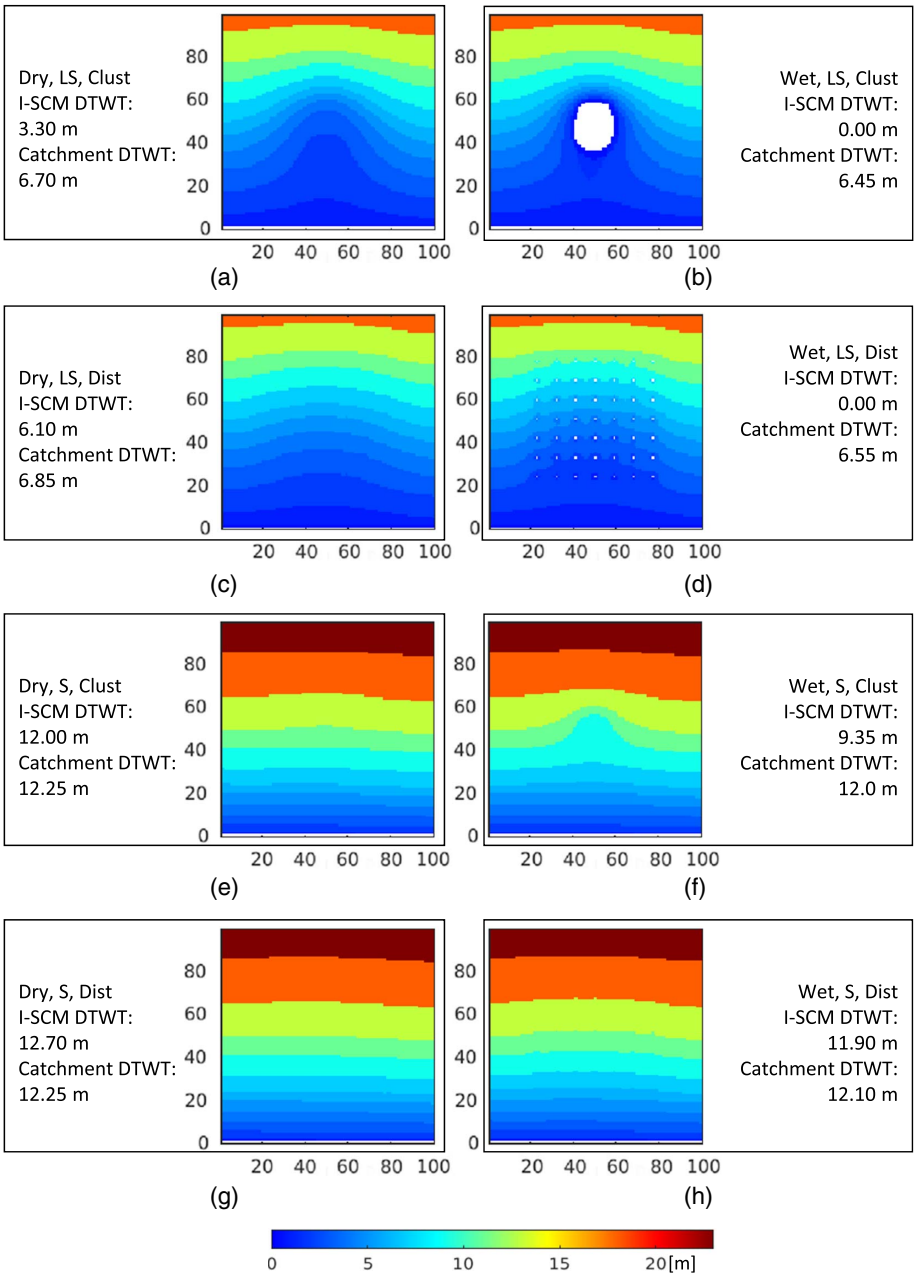

Fig. 6. Depth to water table: (a) dry, loamy sand, clustered; (b) wet, loamy sand, clustered; (c) dry, loamy sand, distributed; (d) wet, loamy sand, distributed; (e) dry, sand, clustered; (f) wet, sand, clustered; (g) dry, sand, distributed; and (h) wet, sand, distributed. White shows locations where groundwater elevation has reached or exceeded surface elevation. Catchment outlet is at origin (bottom left corner). Text shows scenario: loamy sand (LS) or sand (S), and clustered (Clust) or distributed (Dist); average DTWT directly under I-SCMs (I-SCM DTWT), and catchment average DTWT (Catchment DTWT).

Subsurface Flow Drivers

To examine the drivers of flow beneath I-SCMs, hydraulic conductivity, hydraulic gradients, and the product of the two (Darcy flow) for lateral and vertical flow were compared (Fig. 7). The clustered scenario resulted in larger lateral hydraulic conductivities beneath I-SCMs [Fig. 7(a)], as soil moisture was higher beneath clustered compared to distributed I-SCMs (Fig. S1). Lateral hydraulic gradients were towards I-SCMs during long, dry periods and away from I-SCMs during rainfall [Fig. 7(b)]. During days of precipitation, distributed I-SCMs resulted in greater lateral hydraulic gradients directed away from I-SCMs. However, smaller hydraulic conductivities occurred in distributed compared to clustered I-SCMs, with a stronger arrangement effect in loamy sand as compared to sand [Figs. 7(a and b)]. Lateral Darcy flows were greater for the clustered spatial arrangement during both wet and dry periods [Fig. 7(c)].

Drivers of vertical flow were also more sensitive to I-SCM spatial arrangement in the loamy sand than the sand. Vertical hydraulic gradients were consistently away from the I-SCMs (downward) and approached zero during dry periods [Fig. 7(e)]. During precipitation, vertical hydraulic gradients were most strongly downward in the distributed loamy sand scenario and smallest

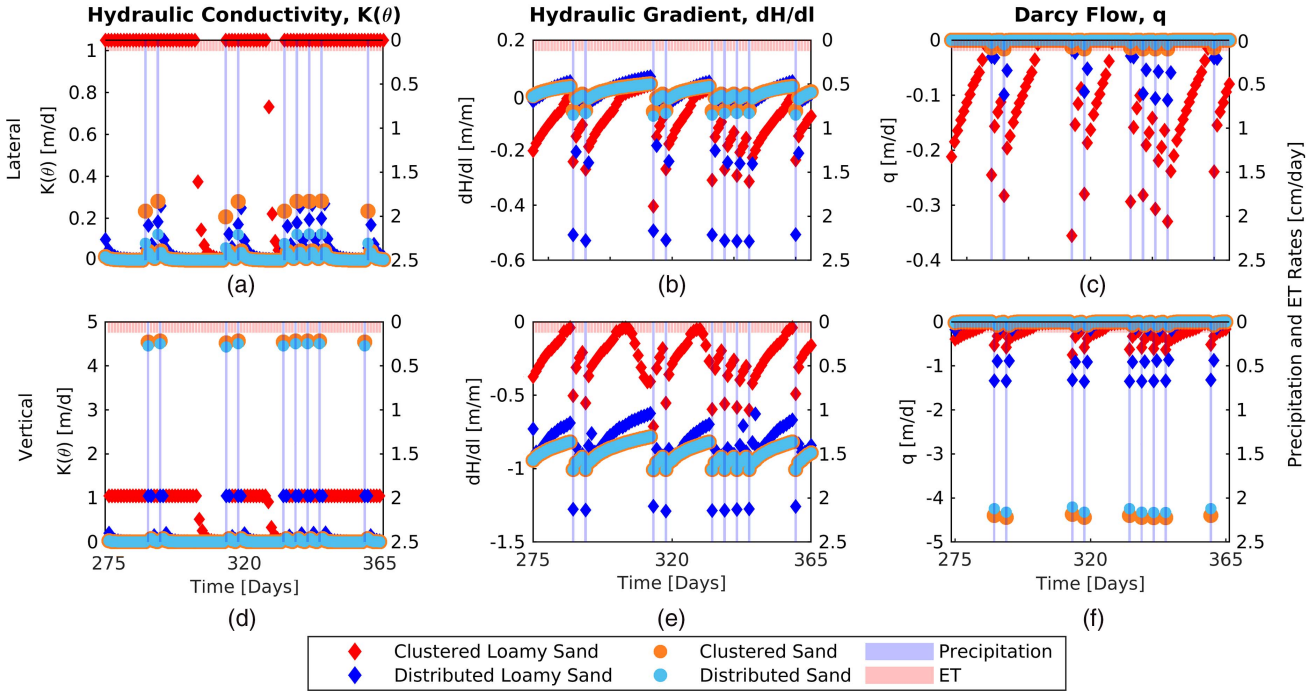

Fig. 7. Medians of subsurface flow drivers within 2.5 m beneath I-SCMs from day 275 through day 365 of simulations: (a) lateral hydraulic conductivity; (b) lateral hydraulic gradient; (c) lateral Darcy flow approximations; (d) vertical hydraulic conductivity; (e) vertical hydraulic gradient; and (f) vertical Darcy flow approximations. Negative values (−) for hydraulic gradient and Darcy flow represent gradients and flows away from I-SCMs, and positive values (+) represent gradients and flows towards I-SCMs.

in the clustered loamy sand scenario. Hydraulic gradients in sand were at or just below the unit downward gradient (−1 m/m), indicating gravity-driven flow. The largest vertical Darcy flow was during days of precipitation in sand, where the hydraulic conductivity was the highest [Fig. 7(f)]. Vertical flow was always greater than lateral flow (Fig. S2). The ratio of lateral to vertical flow increased during wet periods as lateral flow increased with infiltration.

Effects of Evapotranspiration on Results

Loamy sand scenarios resulted in extensive surface ponding for both ET_{low} and ET_{mod} scenarios; therefore, this study focuses on the results from only the sand scenarios to examine the effects of changing ET rates. Steady-state results with the lower ET rates followed the same trends as ET_{high}. For every ET rate, distributed I-SCMs produced greater unsaturated storage and clustered I-SCMs produced greater saturated zone storage. In each case, the differences in unsaturated zone storage between I-SCM spatial arrangements was greater than the difference in saturated storage, so distributed I-SCMs produced greater total subsurface storage. As one would expect, subsurface storage was slightly greater with decreasing ET rates. In general, the results presented for the ET_{high} scenario were representative of the ET_{mod} and ET_{low} scenarios, with three primary differences—(1) baseflow magnitude was higher with lower ET rates, (2) DTWT was smaller with lower ET rates, and (3) with the lowest ET rate and distributed I-SCMs—the recession rate was consistently slower and less dependent on antecedent moisture (Figs. S3 and S4). In general, discharge and recession rates were more sensitive to different ET rates than subsurface behavior, and the changes in hydrologic behavior between soils were much larger than the effects of ET.

Discussion

Dynamic Equilibrium of Transient Simulations

The transient simulations had the same average P-ET as the spin-up simulations, but for the spin-up P-ET was applied as a constant low rate of input. In the transient simulations, unsaturated storage had a decreasing trend over time [Fig. 3(a)], and saturated storage had an increasing trend [Fig. 3(c)]. Although using an average climatic forcing for spin-up is a common approach, the trend seen in the transient simulations indicates that the temporal pattern of P-ET affected storage and discharge magnitudes. Even though there were temporal trends in a given subsurface medium, the differences between spatial arrangements for unsaturated, saturated, and total storage as well as discharge within a subsurface medium remained consistent over time [Figs. 3(b, c, f, and h)], allowing analysis of these differences between spatial arrangements.

Subsurface Storage and Baseflow

While specific magnitudes were presented in the Results section, this section discusses the general relationships that were of primary concern in this work. Distributed I-SCMs always resulted in more unsaturated storage than clustered I-SCMs [Fig. 3(a)], which is also reflected in greater average DTWTs under distributed I-SCMs (Fig. 6). Compared to distributed I-SCMs, clustered I-SCMs led to more cells becoming saturated during precipitation [Figs. 6(b and d)]. As a result, unsaturated storage decreased more during precipitation events and increased more during dry periods for clustered as compared to distributed I-SCMs (Fig. 4). During precipitation, the distributed scenario had more rapid and brief (1–3 days) changes in unsaturated storage compared to the smoother changes with clustered I-SCMs, particularly for loamy

sand [Fig. 3(a)]. This indicates distributed I-SCMs recover infiltration capacity faster with saturated cells more quickly dewatering, compared to clustered I-SCMs.

Spatial arrangement had a stronger effect on unsaturated and saturated storage in loamy sand compared to sand [Figs. 3(b and d)]. Similarly, there were larger differences in unsaturated depth under I-SCMs between arrangements during dry days in loamy sand compared to sand [Figs. 6(a and c) versus Figs. 6(e and g)]. In both subsurface media, the distributed arrangement had infiltration sites that were at higher elevations with deeper DTWTs than clustered I-SCMs. In loamy sand, these distributed I-SCMs with deeper unsaturated zones led to greater downward hydraulic gradients during precipitation [Fig. 7(e)] driving infiltrated water into the deeper unsaturated zone only present at higher elevation I-SCMs. In loamy sand with clustered I-SCMs, vertical hydraulic gradients were small [Fig. 7(e)] as DTWTs under I-SCMs were relatively shallow [Figs. 6(a and b)]. In sand compared to loamy sand, there were even greater DTWTs, but the subsurface medium was so permeable that vertical hydraulic gradients remained small and high hydraulic conductivities led to quicker vertical Darcy flow for both clustered and distributed arrangements.

In silt, there was ponding throughout much of the domain (Table 2). For silt, with distributed I-SCMs 12 of 49 I-SCMs remained unsaturated, whereas in the clustered scenario all I-SCMs saturated. For sand, groundwater mounding was evident in the clustered I-SCM arrangement, but only during precipitation [Fig. 6(f)]. For loamy sand, stormwater infiltration led to groundwater mounding over large parts of the catchment. With the large magnitude of stormwater infiltration modeled, there was surface ponding observed in loamy sand, which receded quickly after precipitation events. Previous studies found that the height of groundwater mounding is very sensitive to subsurface permeability (Carleton 2010; Endreny and Collins 2009) and positioning in topographic sag points (Endreny and Collins 2009). Increases in water table with widespread stormwater infiltration have been found (Barron et al. 2013; Locatelli et al. 2017) as well as localized groundwater mounding that recedes quickly following precipitation events (Machusick et al. 2011; Maimone et al. 2011; Tu and Traver 2019).

The authors expected that distributed I-SCMs would produce more plant available water throughout the root zone because of greater lateral hydraulic gradients beneath I-SCMs. The mean and total plant available water was very similar between spatial arrangements in both sand and loamy sand, but the areas affected were quite different as one might expect (Fig. S1). Clustered I-SCMs in loamy sand had the largest lateral Darcy flow compared to vertical Darcy flow (Fig. S5), whereas distributed I-SCMs in loamy sand produced intermediate ratios and both scenarios in sand produced the smallest ratios. In the clustered loamy sand scenario, the greater lateral to vertical flow, along with more saturated cells occurring under I-SCMs [Fig. 6(b)], produced more plant available water in the region surrounding the I-SCMs than distributed I-SCMs located in the same region (Fig. S1). Cumulative plant available water within I-SCM sites was similar between I-SCM arrangements, but always greater in clustered compared to distributed I-SCMs. These results suggest that clustered I-SCMs have greater potential to provide plants with substantial water over small areas compared to distributed I-SCMs. On the other hand, distributed I-SCMs have greater potential to provide water to plants over a larger area compared to clustered I-SCMs, though the volume available will be less than that in the smaller area under clustered I-SCMs. The magnitude of plant available water was quite similar between scenarios, but the areas affected were quite different. The distribution of plant available water in sand in all ET scenarios was limited to near I-SCMs (Fig. S5).

Assessment of the long-term effect of I-SCM arrangement on baseflow magnitude was limited because the same fluxes in each simulated scenario were applied. This did not allow for soil moisture-limited ET or other climatic feedbacks to be simulated. Based on mass balance, if catchment inputs remain constant and simulations are run to steady state, then outputs (discharge + ET) must be equal to inputs (precipitation). Since ET was applied as a consistent flux, steady-state discharges would be equal. Despite this limitation, running transient simulations that were not at steady state (annual inputs exceeded annual outputs) with consistent forcing between simulations enabled observations about rate of change of subsurface storage and discharge to be made.

It was hypothesized that focused, discrete spatial infiltration, when spatially distributed over larger areas, leads to larger lateral hydraulic gradients beneath I-SCMs, which would then lead to significant lateral subsurface flow away from infiltration sites, lower episodic recharge and baseflow, and increased storage. The distributed I-SCM arrangement did produce larger lateral hydraulic gradients during precipitation events. However, hydraulic conductivities were smaller with distributed I-SCMs and clustered I-SCMs maintained larger lateral gradients during interevent periods. This resulted in more lateral flow with clustered I-SCMs during all times except very dry periods where flow was small under both spatial arrangements [Fig. 7(c)]. While gradients towards I-SCMs were observed during long dry periods, these gradients were likely a result of applying a large and consistent ET rate. If climatic-driven ET and soil-moisture feedbacks had been simulated, it would be expected that gradients towards I-SCMs would be smaller. Distributed I-SCMs did lead to less recharge and increased storage, but this is attributed to greater average depth to water tables under distributed I-SCMs as opposed to more lateral flow. The hypothesized effect on baseflow was not observed. Long-term and episodic baseflow magnitudes were similar between spatial arrangements, but in sand, timing and recession of baseflow response to precipitation were dependent on antecedent precipitation [Figs. 3(g), 4, and 5]. It should also be noted that while I-SCM processes are often considered to be 1D in nature, there can be significant later redistribution of infiltrated water.

Previous observational findings in a catchment developed with a distributed, high spatial density of I-SCMs and 0% effective imperviousness were that baseflow increased during development with reductions in ET (Bhaskar et al. 2016b) as the infiltrated stormwater rapidly became recharge (Bhaskar et al. 2018). The rapid translation of recharge to baseflow is a characteristic of high diffusivity (transmissivity divided by specific yield) aquifers. While I-SCMs will likely help mitigate the effects of development on storm response in the stream, this work indicates that high diffusivity aquifers are not well suited to alterations of subsurface storage or baseflow magnitude with I-SCM spatial arrangement because infiltrated water quickly becomes recharge and moves through the aquifer despite the spatial arrangement. Instead, management of subsurface storage and baseflow magnitude in high diffusivity aquifers may counteract the reductions in ET with use of harvest-based SCMs.

Management Implications

These findings are based on the described model setup, which used idealized conditions to test the effects of arrangements of concentrated stormwater infiltration. Management implications of these findings for optimal spatial arrangement of infiltration-based stormwater control measures (I-SCMs) depend on management goals and should also consider the local physical environment (e.g., soil, slope, climate). Although infiltration of stormwater is sometimes

thought of as water removal (i.e., out of sight out of mind), all stormwater infiltration does not have this same result. More spatially distributed arrangements of I-SCMs lead to longer-term retention of infiltrated water in the subsurface and availability of water in the unsaturated zone for plant uptake over larger areas. In contrast, if increased groundwater recharge is desired, then more clustered I-SCMs would achieve this goal. In areas dependent on groundwater as a water resource, placing clustered or large single I-SCMs may be ideal (in areas void of infrastructure that may be damaged by mounding). In some cities, I-SCMs are subject to regulation that limits stormwater ponding duration. This work has shown that these areas will want to emphasize minimizing the lateral interaction of infiltrated water between I-SCMs to encourage greater infiltration capacity and quicker drawdown rates. These areas will also want to implement I-SCMs in areas with deeper groundwater tables to maintain greater hydraulic gradients that will encourage quicker drawdown.

In low-permeability aquifers, varying I-SCM arrangement is more likely to affect subsurface storage, including plant available water and partitioning between unsaturated and saturated zones, than baseflow. The effect of I-SCM arrangement on plant available water may be taken advantage of in low-permeability aquifers to reduce subsurface storage by placement of vegetation close to I-SCMs. In aquifers with low infiltration capacity, more distributed I-SCMs provide better opportunities to infiltrate stormwater. In extreme cases, large-scale infiltration of stormwater in very low-permeability subsurface media will lead to widespread groundwater mounding and surface ponding. High-permeability aquifers offer less opportunity to manipulate catchment storage by I-SCM placement, but more opportunity to alter baseflow timing and recession behavior. In these aquifers, if more consistent baseflow is desired (e.g., for downstream water supply), distributed I-SCMs are appropriate, but if more dynamic baseflow is desired (e.g., occasional longer duration high flows or low flows for fish rearing or recruitment), then clustered I-SCMs are better suited. More distributed I-SCMs will help reduce the contribution of baseflow to streamflow when the stream is receiving a quick storm response and, thus, can reduce the magnitude of peak flow in response to storms. If single large I-SCMs or more clustered I-SCMs are required, then water should be infiltrated farther from the stream where possible to avoid synchronizing baseflow and overland flow responses.

Conclusions

Infiltration-based low-impact development is an increasingly common approach to mitigating effects of urbanization on streams and catchment-scale hydrologic function. This study investigated how spatial arrangement (clustered versus distributed) of I-SCMs affect subsurface storage and baseflow using a fully distributed physically based watershed model, ParFlow, to simulate two spatial arrangements of I-SCMs in three subsurface media with three ET rates. Here, general patterns of differences between stormwater infiltration arrangements are summarized by the following research questions:

1. Distributed I-SCMs encouraged greater unsaturated zone storage and total subsurface storage whereas clustered I-SCMs led to greater saturated zone storage. Baseflow response to precipitation is sensitive to the arrangement of I-SCMs in high permeability aquifers, and in such cases, clustered I-SCMs are more sensitive to antecedent precipitation compared to distributed I-SCMs and produce more variable baseflow responses. During drier times, if I-SCMs are centered about the same location clustered I-SCMs promote larger magnitude baseflow, whereas with greater antecedent precipitation, distributed I-SCMs promote larger magnitude baseflow.
2. During precipitation events, more clustered arrangements led to larger lateral flow away from I-SCMs than more distributed arrangements, as larger hydraulic conductivities outweighed smaller hydraulic gradients. Distributed I-SCMs produced greater vertical flow than clustered I-SCMs.
3. Results showed baseflow is more responsive to I-SCM spatial arrangement in high-permeability aquifers whereas subsurface storage and its partitioning between unsaturated and saturated zones are more responsive in lower permeability aquifers.

This study has clearly shown that managers should be considering spatial arrangement of stormwater infiltration to meet goals for managing aquifer storage, plant available water, and baseflow. Future work should investigate soil moisture-limited ET, and other climatic feedbacks and their implications for using vegetation to manage urban hydrology.

Data Availability Statement

The following data, models, or code generated or used during the study are available in a repository or online [Choat (2019). ParFlow: Spatial arrangement of stormwater infiltration affects subsurface storage and baseflow, HydroShare, http://www.hydroshare.org/resource/c4774f2ed6124417971c3adb845965a4]. All input files for running spin-up and transient simulations, the main executable files for each simulated scenario, and the main files used for post-processing are included.

Acknowledgments

The authors gratefully acknowledge the helpful comments by Michael Ronayne and Ryan Bailey and anonymous reviewers. This work was partially supported by the USDA National Institute of Food and Agriculture, Hatch project 1015939. This work utilized the RMACC Summit supercomputer (Anderson et al. 2017), which is supported by the National Science Foundation (awards ACI-1532235 and ACI-1532236), the University of Colorado Boulder, and Colorado State University. The Summit supercomputer is a joint effort of the University of Colorado Boulder and Colorado State University.

Supplemental Materials

Figs. S1–S5 are available online in the ASCE Library (www.ascelibrary.org).

References

Anderson, J., P. J. Burns, D. Milroy, P. Ruprecht, T. Hauser, and H. J. Siegel. 2017. "Deploying RMACC summit: An HPC resource for the Rocky Mountain region." In *Proc., Practice and Experience in Advanced Research Computing 2017 on Sustainability, Success and Impact—PEARC17*, 1–7. New Orleans, LA: ACM Press.

Ashby, S. F., and R. D. Falgout. 1996. "A parallel multigrid preconditioned conjugate gradient algorithm for groundwater flow simulations." *Nucl. Sci. Eng.* 124 (1): 145–159. https://doi.org/10.13182/NSE96-A24230.

Barnes, M. L., C. Welty, and A. J. Miller. 2016. "Global topographic slope enforcement to ensure connectivity and drainage in an urban terrain." *J. Hydrol. Eng.* 21 (4): 06015017. https://doi.org/10.1061/(ASCE)HE.1943-5584.0001306.

Barron, O., A. Barr, and M. Donn. 2013. "Effect of urbanisation on the water balance of a catchment with shallow groundwater." *J. Hydrol.* 485 (Apr): 162–176. https://doi.org/10.1016/j.jhydrol.2012.04.027.

Bhaskar, A. S., L. Beesley, M. J. Burns, T. D. Fletcher, P. Hamel, C. E. Oldham, and A. H. Roy. 2016a. "Will it rise or will it fall? Managing the complex effects of urbanization on base flow." *Freshwater Sci.* 35 (1): 293–310. https://doi.org/10.1086/685084.

Bhaskar, A. S., D. M. Hogan, and S. A. Archfield. 2016b. "Urban base flow with low impact development." *Hydrol. Processes* 30 (18): 3156–3171. https://doi.org/10.1002/hyp.10808.

Bhaskar, A. S., D. M. Hogan, J. R. Nimmo, and K. S. Perkins. 2018. "Groundwater recharge amidst focused stormwater infiltration." *Hydrol. Processes* 32 (13): 2058–2068. https://doi.org/10.1002/hyp.13137.

Bhaskar, A. S., and C. Welty. 2015. "Analysis of subsurface storage and streamflow generation in urban watersheds." *Water Resour. Res.* 51 (3): 1493–1513. https://doi.org/10.1002/2014WR015607.

Bonneau, J., T. D. Fletcher, J. F. Costelloe, and M. J. Burns. 2017. "Stormwater infiltration and the 'urban karsti': A review." *J. Hydrol.* 552 (Sep): 141–150. https://doi.org/10.1016/j.jhydrol.2017.06.043.

Carleton, G. B. 2010. *Simulation of groundwater mounding beneath hypothetical stormwater infiltration basins*. Washington, DC: USGS.

Choat, B. 2019. "ParFlow: Spatial arrangement of stormwater infiltration affects subsurface storage and baseflow." *HydroShare*. Accessed August 12, 2020. http://www.hydroshare.org/resource/c4774f2ed6124417971c3adb845965a4.

Denich, C., and A. Bradford. 2010. "Estimation of evapotranspiration from bioretention areas using weighing lysimeters." *J. Hydrol. Eng.* 15 (6): 522–530. https://doi.org/10.1061/(ASCE)HE.1943-5584.0000134.

Dingman, S. L. 2015. *Physical hydrology*. Long Grove, IL: Waveland Press.

Ebrahimian, A., B. Wadzuk, and R. Traver. 2019. "Evapotranspiration in green stormwater infrastructure systems." *Sci. Total Environ.* 688 (Oct): 797–810. https://doi.org/10.1016/j.scitotenv.2019.06.256.

Endreny, T., and V. Collins. 2009. "Implications of bioretention basin spatial arrangements on stormwater recharge and groundwater mounding." *Ecol. Eng.* 35 (5): 670–677. https://doi.org/10.1016/j.ecoleng.2008.10.017.

Ferguson, B. K. 1990. "Role of the long-term water balance in management of stormwater infiltration." *J. Environ. Manage.* 30 (3): 221–233. https://doi.org/10.1016/0301-4797(90)90003-F.

Gupta, S., A. Singh, and A. Ranaivoson. 2004. "Moisture retention characteristics of base and sub-base materials." Accessed October 29, 2018. https://conservancy.umn.edu/bitstream/handle/11299/1124/200506.pdf?sequence=1&isAllowed=y.

Hamel, P., E. Daly, and T. D. Fletcher. 2013. "Source-control stormwater management for mitigating the impacts of urbanisation on baseflow: A review." *J. Hydrol.* 485 (Apr): 201–211. https://doi.org/10.1016/j.jhydrol.2013.01.001.

Hamel, P., and T. D. Fletcher. 2014. "Modelling the impact of stormwater source control infiltration techniques on catchment baseflow." *Hydrol. Processes* 28 (24): 5817–5831. https://doi.org/10.1002/hyp.10069.

Hickman, J., B. Wadzuk, and R. Traver. 2011. "Evaluating the role of evapotranspiration in the hydrology of a bioinfiltration basin using a weighing lysimeter." In *Proc., 2011 World Environmental and Water Resources Congress*. Reston, VA: ASCE.

Hopkins, K. G., A. S. Bhaskar, S. A. Woznicki, and R. M. Fanelli. 2020. "Changes in event-based streamflow magnitude and timing after suburban development with infiltration-based stormwater management." *Hydrol. Processes* 34 (2): 387–403. https://doi.org/10.1002/hyp.13593.

Jefferson, A. J., A. S. Bhaskar, K. G. Hopkins, R. Fanelli, P. M. Avellaneda, and S. K. McMillan. 2017. "Stormwater management network effectiveness and implications for urban watershed function: A critical review." *Hydrol. Processes* 31 (23): 4056–4080. https://doi.org/10.1002/hyp.11347.

Jones, J. E., and C. S. Woodward. 2001. "Newton-Krylov-multigrid solvers for large-scale, highly heterogeneous, variably saturated flow problems." *Adv. Water Resour.* 24 (7): 763. https://doi.org/10.1016/S0309-1708(00)00075-0.

Kollet, S. J., and R. M. Maxwell. 2006. "Integrated surface–groundwater flow modeling: A free-surface overland flow boundary condition in a parallel groundwater flow model." *Adv. Water Resour.* 29 (7): 945–958. https://doi.org/10.1016/j.advwatres.2005.08.006.

Li, C., T. D. Fletcher, H. P. Duncan, and M. J. Burns. 2017. "Can stormwater control measures restore altered urban flow regimes at the catchment scale?" *J. Hydrol.* 549 (Jun): 631–653. https://doi.org/10.1016/j.jhydrol.2017.03.037.

Locatelli, L., O. Mark, P. S. Mikkelsen, K. Arnbjerg-Nielsen, A. Deletic, M. Roldin, and P. J. Binning. 2017. "Hydrologic impact of urbanization with extensive stormwater infiltration." *J. Hydrol.* 544 (Jan): 524–537. https://doi.org/10.1016/j.jhydrol.2016.11.030.

Machusick, M., A. Welker, and R. Traver. 2011. "Groundwater mounding at a storm-water infiltration BMP." *J. Irrig. Drain. Eng.* 137 (3): 154–160. https://doi.org/10.1061/(ASCE)IR.1943-4774.0000184.

Maimone, M., D. E. O'Rourke, J. O. Knighton, and C. P. Thomas. 2011. "Potential impacts of extensive stormwater infiltration in Philadelphia." *Environ. Eng. Appl. Res. Pract.* 14: 1–12.

Maxwell, R. M. 2013. "A terrain-following grid transform and preconditioner for parallel, large-scale, integrated hydrologic modeling." *Adv. Water Resour.* 53 (Mar): 109–117. https://doi.org/10.1016/j.advwatres.2012.10.001.

Newcomer, M. E., J. J. Gurdak, L. S. Sklar, and L. Nanus. 2014. "Urban recharge beneath low impact development and effects of climate variability and change." *Water Resour. Res.* 50 (2): 1716–1734. https://doi.org/10.1002/2013WR014282.

Poff, N. L., J. D. Allan, M. B. Bain, J. R. Karr, K. L. Prestegaard, B. D. Richter, R. E. Sparks, and J. C. Stromberg. 1997. "The natural flow regime." *BioScience* 47 (11): 769–784. https://doi.org/10.2307/1313099.

Price, K. 2011. "Effects of watershed topography, soils, land use, and climate on baseflow hydrology in humid regions: A review." *Prog. Phys. Geogr.* 35 (4): 465–492. https://doi.org/10.1177/0309133311402714.

Reitz, M., W. E. Sanford, G. B. Senay, and J. Cazenas. 2017. "Annual estimates of recharge, quick-flow runoff, and evapotranspiration for the contiguous U.S. using empirical regression equations." *J. Am. Water Resour. Assoc.* 53 (4): 961–983.

Rose, S., and N. E. Peters. 2001. "Effects of urbanization on streamflow in the Atlanta area (Georgia, USA): A comparative hydrological approach." *Hydrol. Processes* 15 (8): 1441–1457. https://doi.org/10.1002/hyp.218.

Sasidharan, S., S. A. Bradford, J. Šimuunek, and S. R. Kraemer. 2019. "Drywell infiltration and hydraulic properties in heterogeneous soil profiles." *J. Hydrol.* 570 (Mar): 598–611. https://doi.org/10.1016/j.jhydrol.2018.12.073.

Schaap, M. G., F. J. Leij, and M. T. van Genuchten. 2001. "Rosetta : A computer program for estimating soil hydraulic parameters with hierarchical pedotransfer functions." *J. Hydrol.* 251 (3–4): 163–176. https://doi.org/10.1016/S0022-1694(01)00466-8.

Shields, C., and C. Tague. 2015. "Ecohydrology in semiarid urban ecosystems: Modeling the relationship between connected impervious area and ecosystem productivity." *Water Resour. Res.* 51 (1): 302–319. https://doi.org/10.1002/2014WR016108.

Staudinger, M., M. Stoelzle, F. Cochand, J. Seibert, M. Weiler, and D. Hunkeler. 2019. "Your work is my boundary condition!" *J. Hydrol.* 571 (Apr): 235–243. https://doi.org/10.1016/j.jhydrol.2019.01.058.

Tu, M.-C., and R. Traver. 2019. "Water table fluctuation from green infrastructure sidewalk planters in Philadelphia." *J. Irrig. Drain. Eng.* 145 (2): 05018008. https://doi.org/10.1061/(ASCE)IR.1943-4774.0001369.

van Genuchten, M. T. 1980. "A closed-form equation for predicting the hydraulic conductivity of unsaturated soils1." *Soil Sci. Soc. Am. J.* 44 (5): 892. https://doi.org/10.2136/sssaj1980.03615995004400050002x.

Walsh, C. J., A. H. Roy, J. W. Feminella, P. D. Cottingham, and P. M. Groffman. 2005. "The urban stream syndrome: Current knowledge and the search for a cure." *J. North Am. Benthological Soc.* 24 (3): 706–723. https://doi.org/10.1899/04-028.1.

Wiles, T. J., and J. M. Sharp Jr. 2008. "The secondary permeability of impervious cover." *Environ. Eng. Geosci.* 14 (4): 251–265. https://doi.org/10.2113/gseegeosci.14.4.251.

Winston, R. J., J. D. Dorsey, and W. F. Hunt. 2016. "Quantifying volume reduction and peak flow mitigation for three bioretention cells in clay soils in northeast Ohio." *Sci. Total Environ.* 553 (May): 83–95. https://doi.org/10.1016/j.scitotenv.2016.02.081.

Woods, R. A., M. Sivapalan, and J. S. Robinson. 1997. "Modeling the spatial variability of subsurface runoff using a topographic index." *Water Resour. Res.* 33 (5): 1061–1073. https://doi.org/10.1029/97WR00232.